MDPI

Article

Development of a time correction algorithm for a precise synchronization of a free running Rubidium clock with the GPS time

Claire Dalmazzone [1,†,‡], Mathieu Guigue [2,‡], Lucile Mellet [2,‡], Boris Popov [2,‡], Stefano Russo [2,‡] and Vincent Voisin [2,*]

[1] Affiliation 1; e-mail@e-mail.com
[2] Affiliation 2; e-mail@e-mail.com
* Correspondence: e-mail@e-mail.com; Tel.: (optional; include country code; if there are multiple corresponding authors, add author initials) +xx-xxxx-xxx-xxxx (F.L.)
† Current address: Affiliation 3.
‡ These authors contributed equally to this work.

Abstract: We present results of our study devoted to development of a time correction algorithm needed to precisely synchronize a free running Rubidium clock with the Universal Time Coordinated (UTC). This R&D is performed in view of the Hyper-Kamiokande (HK) [1] experiment currently under construction in Japan, which requires a synchronization with UTC and between its different experimental sites with a precision better than 100 ns. We use a Global Navigation Satellite Systems (GNSS) receiver to compare and correct a 1 PPS signal, generated by a free running Rubidium clock, to the Global Positioning System (GPS) time signals. We fit the Rubidium vs GPS PPS residuals data with polynomials functions of time over a certain integration time window to extract a correction of the free running Rubidium signal in offline or online mode. In online mode, the latest fits results are used to correct the Rubidium signal until a new comparison to GPS becomes available. We show that with an integration time window of PPS residuals data of around 10^4 seconds, we can correct the free running Rubidium signal for the frequency random walk noise so that the PPS residuals stay within a ± 5 ns window in both offline or online correction mode.

Keywords: precise timing; atomic clock; Rb; PHM; GNSS; GPS; UTC

1. Introduction

A precise synchronization of a free running atomic clock signal with the Universal Time Coordinated (UTC) or with another signal is a necessity in many applications, particularly in physics experiments including several experimental sites that must be synchronized. A good example is long baseline neutrino oscillation experiments, like OPERA [2] (2006-2012), T2K [3] (from 2010) and NOvA [4] (from 2014), where a beam of neutrinos is produced and characterized in a first experimental site and detected, after several hundreds of kilometers of propagation, at another site to measure the change of the beam properties. Several next generation long baseline neutrino experiments are being built at the moment, like Hyper-Kamiokande (HK) [1] that plans to start taking data in 2027 and DUNE [5] that should begin sometime after 2029. These experiments require a synchronization between the different experimental sites. For HK for instance, this requirement is of 100 ns or better. Moreover, multi-messenger programs that plan to compare different components of astrophysical events [6] (e.g.: gamma-ray bursts, gravitational waves, neutrino emissions of supernovae, etc.) require a synchronization with UTC of different experiments located all over the world. For instance, to enter the SuperNova Early Warning System (SNEWS) network [7], a synchronization to UTC better than 100 ns is needed.

Many physics experiments use atomic oscillators as frequency references because of their good short term stability. One of the reference oscillators available are Rubidium

Citation: Dalmazzone, C.; Guigue, M.; Mellet, L.; Popov, B.; Russo, S.; Voisin, V. Title. *Journal Not Specified* **2024**, *1*, 0. https://doi.org/

Received:
Revised:
Accepted:
Published:

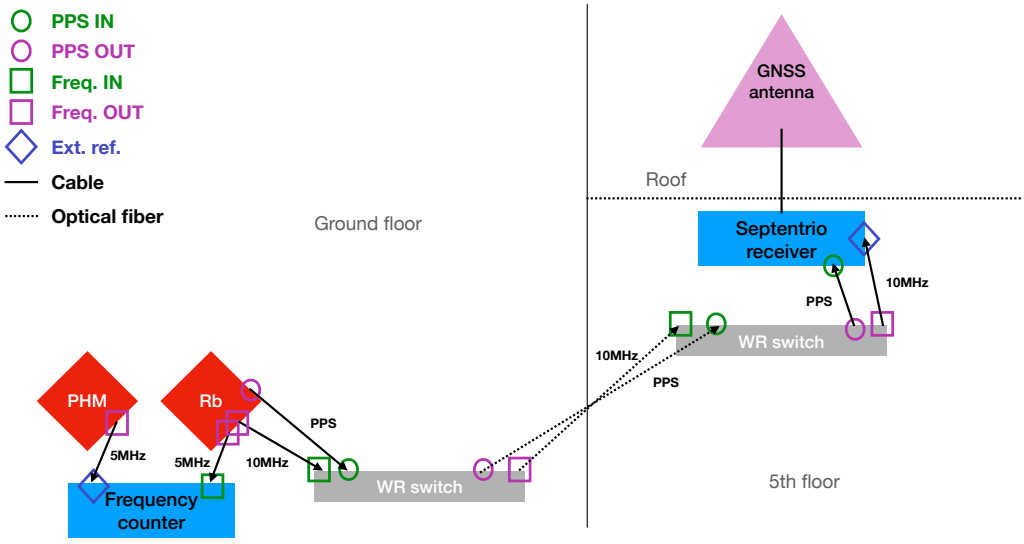

Figure 1. Experimental setup used in this work. Part of the equipment is installed at the ground floor and the other part at the fifth floor. The relevant signals generated at the ground floor are transported to the fifth floor via optical fibers with the White Rabbit (WR) protocol. This particular setup mimics what could happen in underground experiments where the clock signal would be generated underground whereas the GNSS antenna and receiver would be above-ground.

clocks, which are generally chosen for affordability as it was the case for the T2K [8] and Super-Kamiokande [9] timing systems. However, Rubidium clocks signals usually drift away from a stable reference because of frequency drift and random walk. For synchronization to UTC, this drift usually needs to be prevented or corrected. A common solution is to phase-lock the clock to an external Global Navigation Satellite Systems (GNSS) signal, with a chosen integration time window long enough in order not to deteriorate the short term stability of the clock. However, it presents some drawbacks like the fact that the user has little control on the setup. In case of problems (like jumps in the time signal), it is difficult to understand where they come from (GNSS signals, receiver, the master clock, etc.) and to assess the uncertainty on the synchronization to UTC. The R&D work presented in this paper and introduced in [10] is focused on designing and characterizing an alternative method that allows more freedom to the user and a better understanding of the process. It is based on known metrology techniques [11,12]. The proposed method uses a free running atomic clock to derive a time signal that is corrected in post-processing using comparisons to the GNSS signals. In that way, we can safeguard all the information (the raw signal, the comparisons to GNSS signals, the derived correction etc.) and apply the correction in either online (during the data-acquisition) or offline modes.

2. Materials and Methods

2.1. Experimental setup

The experimental setup that we used is schematized in Figure 1. It is located at the Pierre and Marie Curie (Jussieu) campus of the Sorbonne University in Paris. The setup consists of two main parts: one represents the timing generation and correction setup, that could be reproduced in physics experiments, and the second part is related to testing the efficiency of the correction method. In the first part a Rubidium clock (Rb) in free running mode, at the ground floor of the laboratory, generates a Pulse Per Second (PPS) and a 10 MHz signal that are transported to the fifth floor with the White Rabbit (WR) protocol. The 10 MHz signal is used by a GNSS receiver as a reference for its internal clock. The receiver is used to measure comparisons between the GNSS satellites signals provided by the antenna on the roof (above the fifth floor) and the Rubidium clock PPS signal. This

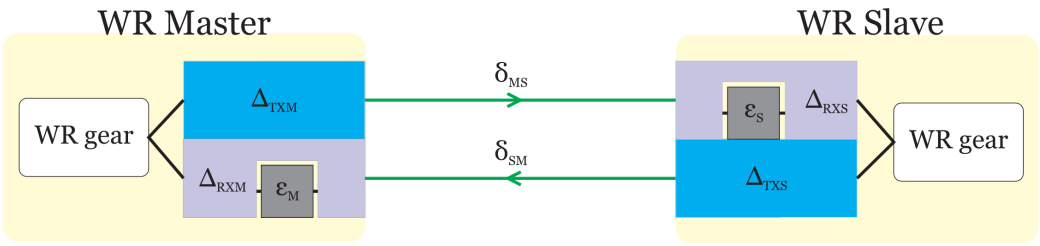

Figure 2. White Rabbit link model, from [15]

physical distance between the time generation part and the receiver was done on purpose to mimic what would happen in many physics experiments. Indeed, in Hyper-Kamiokande, the Rubidium clock would be placed inside a mountain where a cavern has been dug to host the detector whereas the receiver would have to be placed outside in a valley. The second part of our experimental setup is contained in the experimental room at the ground floor and its purpose is to validate the performance of the method, it would not be reproduced in the final setup in Hyper-Kamiokande. It consists in a frequency counter measuring the frequency of the 5 MHz signal generated by the Rubidium clock. The reference for the internal clock of the counter is an external 5 MHz signal generated by a Passive Hydrogen Maser (PHM).

2.1.1. Rubidium clock

The Rubidium clock used is the FS725 Rubidium Frequency Standard sold by Stanford Research Systems integrating a rubidium oscillator of the PRS10 model. It provides two 10 MHz and one 5 MHz signals with very low phase white noise and the stability measured via the Allan Standard Deviation (ASD) [13] at 1 s of $\sim 2 \times 10^{-11}$ (see Figure 9). It also provides a PPS output with a jitter of less than 1 ns. Its 20 years aging was estimated to less than 5×10^{-9} and the Mean Time Before Failure is over 200,000 hours. It can also be phase-locked to an external 1 PPS reference, like the GPS for instance. The FS725 is installed at the ground floor of our laboratory and its 10 MHz and 1 PPS output are transported to the GNSS receiver at the fifth floor.

2.1.2. White Rabbit switches

The White Rabbit (WR) project [14] is a collaborative effort involving CERN, the GSI Helmholtz Centre for Heavy Ion Research, and other partners from academia and industry. Its primary objective is to develop a highly deterministic Ethernet-based network capable of achieving sub-nanosecond accuracy in time transfer. Initially, this network was implemented for distributing timing signals for control and data acquisition purposes at CERN's accelerator sites.

The experimental setup described uses two WR switches to propagate the Rubidium clock PPS and frequency signals from the ground floor to the fifth floor with great precision.

Calibration

In order to achieve a sub-nanosecond synchronization between switches a calibration of the link must be done. A White Rabbit link between two devices is characterized by specific hardware delays and fiber propagation latencies.

Each WR Master and WR Slave possesses fixed transmission and reception delays (ΔT_{XM}, ΔRXM, ΔT_{XS}, ΔRXS). These delays are the cumulative result of various factors such as SFP transceiver, PCB trace, electronic component delays, and internal FPGA chip delays. Additionally, there is a reception delay on both ends caused by aligning the recovered clock signal to the inter-symbol boundaries of the data stream, referred to as the bitslide value (ϵ_M and ϵ_S in Figure 2).

We can see the results of calibration process in Figure 3, the difference of PPS between the two nodes change from 165 ps to 60 ps (with a 100 m fiber).

Figure 3. Difference of PPS before and after calibration

REFIMEVE

Note that the LPNHE, as a part of the T-REFIMEVE network [16,17], has access through a dedicated switch to the official French realization of the UTC, called UTC(OP) (for Observatoire de Paris), transported from the SYRTE laboratory via White Rabbit protocol. REFIMEVE is a French national research infrastructure aiming at the dissemination of French legal time and frequency standards to more than 30 research laboratories and research infrastructures all over France. The reference signals originate from LNE-SYRTE and are mainly transported over the optical fiber backbone of RENATER, the French National Research and Education Network. The UTC(OP) signal was not used in the final experimental setup because we do not foresee to have access to such a high precision signal in HK experiment.

2.1.3. Septentrio GNSS antenna and receiver

We use the Septentrio PolaNt Choke ring GNSS antenna that supports GNSS signals from many satellite constellations including GPS, GLONASS, Galileo, BeiDou and others. In this work, we restrict the analysis to the GPS signals but it can easily be generalized to any subset of constellations. The antenna position has been previously measured to a precision better than 6 mm by trilateration (not triangulation) with the help of a web-based service provided by Canadian gouvernment [26]. We use a Septentrio PolaRx5 GNSS reference receiver as a timing receiver to compare the GNSS signals to the Rubidium 1 PPS. First, when the receiver is switched on with, as input, the Rubidium 1 PPS signal transported via White Rabbit, the phase of the receiver internal clock will lock to this 1 PPS. The internal clock is also tuned on the external reference that we put: the 10 MHz signal coming via White Rabbit from the Rubidium clock. The Septentrio receiver thus provides one point every 16 min which is the middle point of the linear function fitted from the 13 min of data from the beginning of this 16 min time window. The results of the measurements are safeguarded using the CGGTTS file format [18].

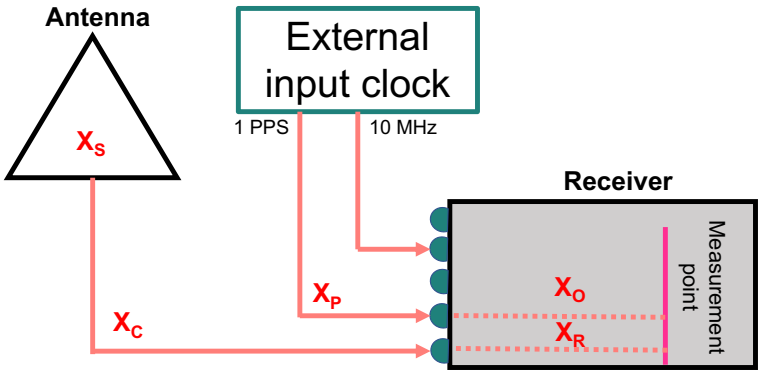

Figure 4. Delays to consider for the selected GNSS receiver+antenna pair, from [19]

Before taking measurements, the whole system has been calibrated against official reference signals from the SYRTE laboratory. As it can be seen in Figure 4, the following delays need to be measured and taken into account during operation [20]. The calibration consists in measuring these:

- X_S: internal delay inside the antenna, frequency dependent
- X_C: delay caused by the antenna cable
- X_R: internal delay of the receiver for the antenna signal, frequency dependent
- X_P: in case an external signal is given in input, connection cable delay
- X_O: in case an external signal is given in input, internal receiver delay between external 1 PPS and internal clock

X_S and X_R depend on the GNSS frequency that is being read, meaning it is specific to each frequency of each GNSS constellation. The calibration was here performed for both GPS and Galileo constellations, each having two available frequencies. The cable delays X_C and X_P can be evaluated with specific equipment that measures the round-trip time of an injected signal. The dispersion can be measured with the same device. To reproduce the experimental conditions of underground experiments like HK or DUNE where the GNSS antenna is outside, away from the detector, a 100 m cable was used and calibrated. The total cable delay was measured to be 505 ns. The internal delays of the antenna and receiver can only be measured together (for each frequency) as $\text{INTDLY} = X_S + X_R$. This was done through a comparison with OP73, one of the calibrated receivers of SYRTE, and with UTC(OP), the French realization of UTC, as an input to the two receivers. The values of INTDLY found for the two most widely available frequencies of the GPS constellation (L1 and L2) and the Galileo constellation (E1 and E5a) are given in Table 1.

Finally, X_O can be set to 0 thanks to an auto-calibration feature of the selected receiver.

Table 1. Values of INTDLY in ns found for the first antenna+receiver+cable system calibrated at the SYRTE lab against the OP73 station

GPS L1	GPS L2	Galileo E1	Galileo E5a
25.832	22.871	28.242	25.431

The delays X_C, INTDLY, and REFDLY can then be given as parameters of the receiver so that they are automatically handled in any further use of the receiver. Uncertainty on the measured delays were evaluated to 4 ns according to estimations fixed for the employed method. The calibration needs to be re-done for any new antenna+receiver+cable combination.

2.1.4. Passive Hydrogen Maser

A Passive Hydrogen Maser (PHM) from T4 Science was also acquired. Note that this instrument is not available anymore. This clock is approximately 10 times more expensive than a Rubidium clock but is also much more stable. Indeed, the Allan Standard Deviation (ASD) at 1 s is only of $\sim 5 \times 10^{-13}$ and according to the production company, the maximum accumulated drift after 10 years is of 1×10^{-11}. The PHM provides a 1 PPS signal as well as two outputs of 5 MHz, two outputs of 10 MHz, one output of 100 MHz and a sine output of 1 MHz as well as a 2.048 MHz square signal. Here, we use the PHM to generate a "perfect signal" to compare our Rubidium clock signal to.

2.1.5. Frequency counter

The frequency counter is the 53220A model from Keysight Technologies. It has three input channels and an input for an external frequency to use as a reference for its internal clock. The instrument can be used to measure the frequency of a signal input at any of the three channels. The instrument either uses directly its internal oscillator or, if specified by the user, the internal oscillator can be tuned to the external reference frequency. The external reference must be a sine wave with a frequency of 5, 10 or 100 MHz. The resolution of the frequency measurement is set by the user and must range between 10^{15} and 10^{-5} times the expected frequency. The set resolution will determine the integration time window for the measurement called gate-time. The better the resolution, the longer the gate time.

The frequency counter was used to measure the Rubidium clock 5 MHz signal frequency simultaneously to the PPS residuals measurements performed by the Septentrio receiver. The external frequency reference was set to be the 5 MHz signal of the PHM and the resolution was set to 0.01 mHz which corresponds to a relative resolution of 2×10^{-11}. This resolution is good enough to measure the ASD of the Rubidium clock at low averaging times.

2.2. Corrections methods

2.2.1. General principle

To synchronize our clock signal to UTC, we apply a time-dependent correction (quadratic or linear) to the 1 PPS signal generated by the free running Rubidium clock $\phi_{Rb}(t)$. We model the k^{th} portion of the PPS residuals distribution ($dt_{Rb,GNSS}$), defined as the difference between the free running Rb clock and the GNSS signals distribution, as a (one or two degrees) polynomial of time

$$\forall t \in [t_{k-1}, t_k], dt_{Rb,GNSS}(t) = a_k \cdot t^2 + b_k \cdot t + c_k. \quad (1)$$

The coefficients a_k ($a_k = 0$ in case of linear fit), b_k and c_k of the polynomials are extracted from least square polynomial fits of the PPS residuals distributions. The fits of these residuals, obtained from the Septentrio receiver, are performed for every k^{th} time window of length Δt. In other words, we model the Septentrio measurements with a piece-wise polynomial function of time. For the k^{th} time window (between t_k and t_{k+1}), we get the corrected time signal

$$\forall t \in [t_k, t_{k+1}],\ \phi_{Rb,corr}(t) = \phi_{Rb}(t) - a_k \times t^2 - b_k \times t - c_k. \quad (2)$$

The time-length Δt of the pieces (time windows) has to be chosen carefully. In particular, it should be short enough in order to correct for the effect of the frequency random walk of the Rubidium clock but not too short to not deteriorate its good short term stability.

In the following, we consider two types of correction: the offline and the online corrections. The difference between the two methods is illustrated in Figure 5. The offline correction consists in using the Septentrio data from the same time-window as the Rubidium signal we want to correct to extract the a_k, b_k and c_k coefficients. This correction is called offline because it requires the Septentrio data from up to $t_k + \Delta t = t_{k+1}$ to correct

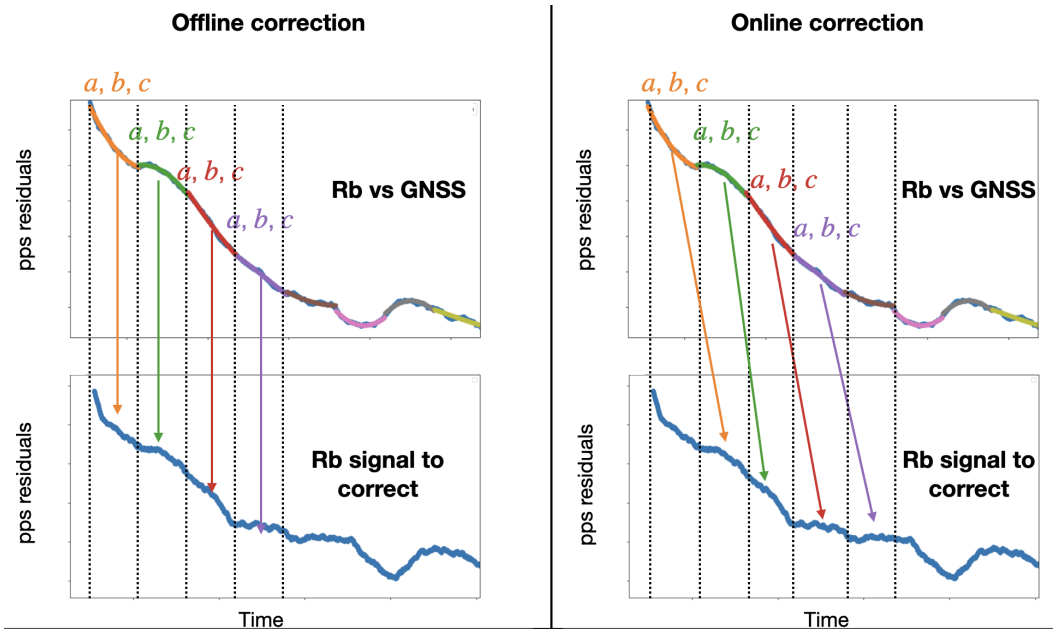

Figure 5. Schematic representation of the offline (left) and online (right) corrections. In the offline correction, we extract the correction coefficients using Rb PPS residuals against GNSS from the same time-window as the data we want to correct. In the online correction, we use Rb PPS residuals against GNSS from the previous time-window with respect to the data interval we want to correct. Only the second correction can be applied in real time as it only requires comparisons with GNSS from the past of the signal we correct.

all the Rb signal between t_k and t_{k+1} so it cannot be performed in real-time (because one would need to wait a time Δt to extract the correction coefficients for the signal at time t_k).

The online correction consists in correcting the Rubidium signal between t_k and t_{k+1} using Septentrio data collected before t_k. One example of online correction is illustrated in Figure 5 where Septentrio data received between $t_{k-1} = t_k - \Delta t$ and t_k are used to correct the Rubidium signal between t_k and $t_{k+1} = t_k + \Delta t$. This method is called online because it can be applied in real time. In the following, we will consider the most frequent possible update of the a_k, b_k and c_k coefficients: they will be updated every time we receive a new data point from the Septentrio receiver (every $\delta t \approx 16$ minutes in our case). This means that we have $t_{k+1} = t_k + \delta t$ so that the a_k, b_k and c_k coefficients are extracted using Septentrio data between $t_k - \Delta t$ and t_k and are used to correct the Rubidium signal between t_k and $t_k + \delta t$. In that particular case every Septentrio data point will have been used in multiple fits, the number depending on the length of the fit time window Δt.

The performance of the correction is evaluated in two ways. First, we look at the stability of the corrected free running Rubidium signal estimated with the Overlapping Allan Standard Deviation (OASD). Then, we also look at the PPS residuals against GPS signal after correction.

2.2.2. Validation of the method with simulations

Before evaluating the performance of our timing system when integrating the correction algorithm, the method was validated on simulated signals [19] in order to isolate the effect and performance of the correction from any measurement effect.

Simulation details

Three types of signal were considered: a perfect PPS to use as a reference to evaluate the performance, a free Rubidium clock PPS and a GNSS PPS. Phase series were simulated and transformed into PPS signals for simplicity. The quadratic drift was not included because it is deterministic and therefore does not require further study for being corrected.

At first order, the clock signal can be modeled by white noise (WN) in both phase and frequency as well as a random walk (RW) noise in frequency. The GNSS can be modeled as pure phase white noise. The OASD of these frequency signals as a function of the averaging time τ can be modeled [21–23] by:

$$OASD(\tau) \cong A_{WNp} \times \tau^{-1} + A_{WNf} \times \tau^{-1/2} + A_{RWf} \times \tau^{+1/2}. \quad (3)$$

The amplitudes A of these main frequency and phase noises were determined through fitting this model (Eq. 3) to the OASD of the data when characterizing our equipment and found to be:

$$\begin{aligned} A_{WNf} &= 7 \times 10^{-12}, \\ A_{RWf} &= 1 \times 10^{-15}, \\ A_{WNp} &= 5 \times 10^{-11}, \end{aligned} \quad (4)$$

for the free Rb clock and for the GNSS signals:

$$\begin{aligned} A_{WNf} &= 0, \\ A_{RWf} &= 0, \\ A_{WNp} &= 2 \times 10^{-9}, \end{aligned} \quad (5)$$

with indices f and p for frequency and phase respectively. Those amplitudes are unit-less because throughout the study presented here we have been using Allan deviations in such a way that they do not have units: they are either variances of frequency ratios or variances of time differences divided by the square of the averaging time.
The equivalent of 10^6 s of data was simulated. To mimic the output of the GNSS receiver, time differences between the simulated Rubidium PPS and the simulated GNSS PPS (Δt^i_{Rb-ref}) are computed every 16 mn[1], taking the average, over that period of time, of differences between each signal for each pulse.

Offline corrections

First, the offline corrections were tested on the simulated data. The OASD curves are obtained using the simulated perfect PPS as reference. In Figure 6, the uncorrected simulated signals of the GPS and the clock are reported in dotted symbols for comparison. The increase of the clock's OASD after $\tau = 10^4$ s due to the random walk is clearly visible. One can see that the OASD of the corrected signals (starred symbols) do eliminate the random walk at longer terms which indicates a success of the correction method. Moreover, one can determine that the ideal length Δt of the correction time windows lies around 10^4 s which corresponds logically to the intersection of the free Rb clock and the GPS signals OASD curves. Indeed, the red curve with a time window of 10560 s shows an ideal combination of the short-term stability of the clock and the absence of random walk at longer scales. On the opposite, the yellow (shorter time window) and light blue (longer time window) curves show respectively a degradation of the short term performance and a remaining random walk component in the region between $\tau = 10^4$ s and the time window length (here 240000 s).

[1] In principle, we should only use 13 mn and discard 3 mn of data to perfectly mimic the receiver's process but this does not impact our results.

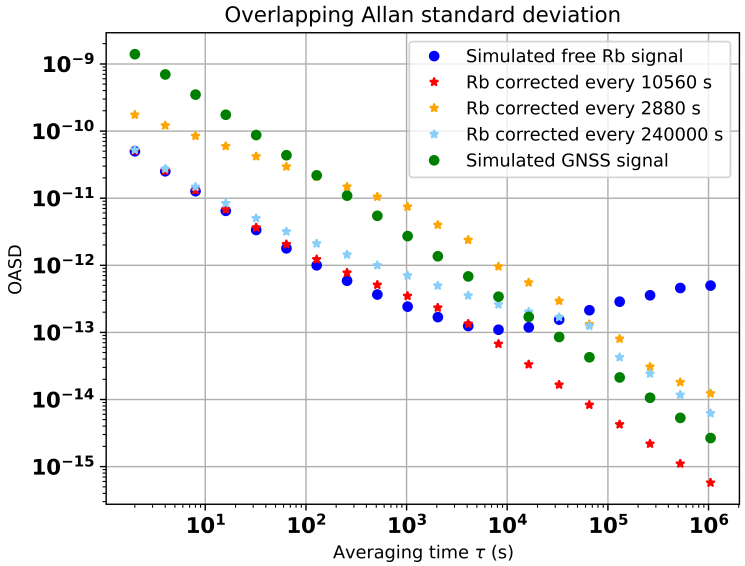

Figure 6. Comparison of overlapping ASD for corrected signals with different time windows

Online corrections

The online correction method was then applied to the simulated data using time series directly and a window length of $\Delta t = 10^4$ s. The results are shown in Figure 7 in red and prove to be just as efficient as the offline correction method to remove the random walk at longer time scales which is the main goal. The overall precision on the long term region (after $\approx 10^3$ s) is as expected slightly degraded compared to the offline correction.

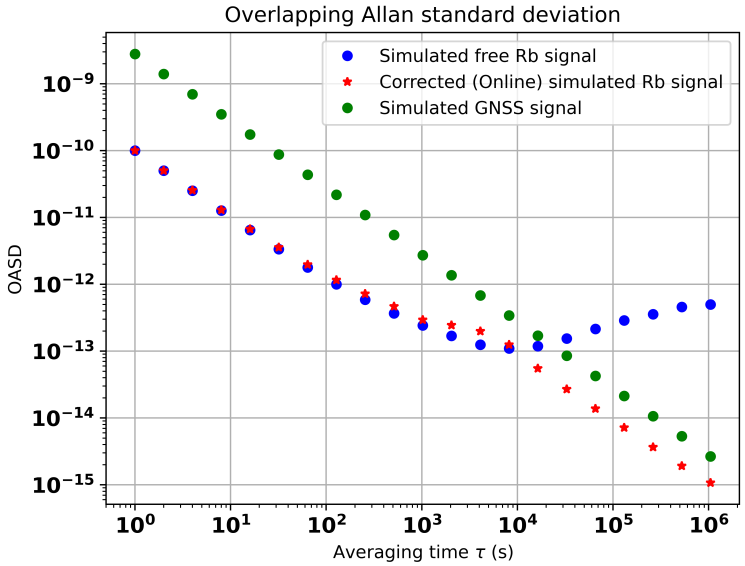

Figure 7. After online corrections at 10^4 s: Overlapping ASD with respect to perfect signal

Conclusion

As a conclusion, it can be said that the application of the correction algorithms to the simulated signals allowed us to validate the chosen correction methods, both the offline and online ones. Indeed, looking at the PPS residuals after correction in Figure 8, one can see that the remaining variations for both methods are well within the experiment's requirements as they stay within a few ns. Over 6 different simulations the remaining variations were found to be for offline and online corrections respectively $\sigma_{Off} = 0.35 \pm 0.05$ ns and $\sigma_{On} = 0.56 \pm 0.05$ ns.

Finally, it is important to note that although this validates the methods for application on data, those are simplified simulations, in particular because only the main noise types are taken into account. As a result, we do expect the algorithms to perform slightly worth on data. More specifically, one thing that can be surprising in the simulation results is that the corrected signal has a better stability than the GNSS signals used for the correction. This can not be the case in real data.

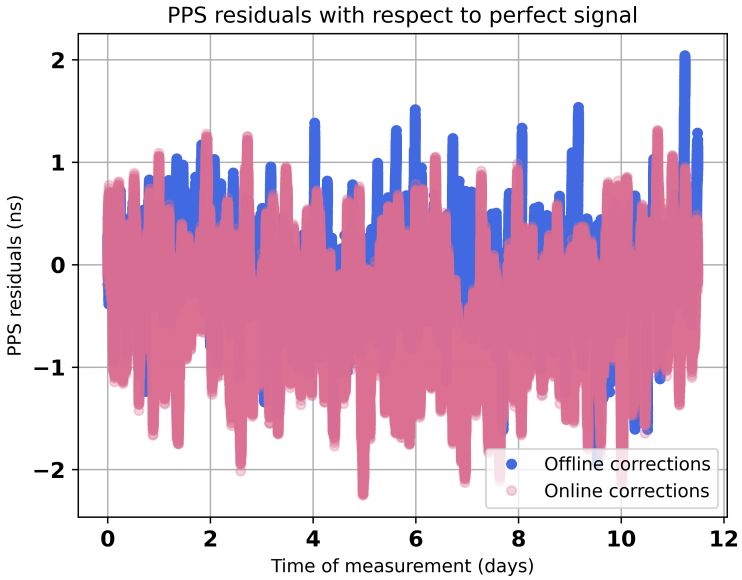

Figure 8. Comparison of time variations for simulated signals corrected with the offline method (blue) or with the sliding interval online method (pink)

2.2.3. Implementation on data

To check the impact of the correction on the Rubidium clock signal, we compare the free running and corrected signal to another more stable clock, like a Passive Hydrogen Maser. The PHM signal plays the role of the perfect signal used for the simulations, while obviously not being perfect. This first difference is to take into account while comparing performances on simulated data to performance on experimental data. In the following, we will also quantify the stability of the Rubidium signal using the OASD of a series of frequency ratios [2] between this signal and the 5 MHz generated by the PHM. Measuring this ratio frequently, like once per second, would allow to also evaluate the very short term stability of the corrected signal which is not possible with the Septentrio measurements that are integrated over 16 minutes. We used the frequency counter to provide every second a measurement of the Rubidium clock 5 MHz frequency f^i_{Rb} taking the PHM 5 MHz generated signal as a frequency reference f_{ref}. We then performed a simultaneous correction of the Rb 1 PPS signal and of this frequency ratio $f^i = f_{Rb}/f_{ref}$ series. Comparing the OASD of the corrected frequency series to the uncorrected one, one can quantify the short term stability after correction while making sure that the random walk was corrected. We can also use this comparison to tune the value of Δt in order to achieve the lowest Allan Standard Deviation possible at all averaging time windows.

3. Results

In this Section, we present the results of the correction of the Rubidium time signal obtained for simultaneous measurements of $\sim$ 50 days with the Septentrio receiver and the frequency counter with PHM 5 MHz signal as a frequency reference. The frequency measurements are divided by the expected value to obtain a series of Rb/PHM frequency ratios. The OASD of such a frequency series is shown in Figure 9. Note that the statistical uncertainties on the estimated OASD, due to the limited number of samples per averaging time, are included as error bars for both curves (Rb and GPS) but they are too small to be visible. Indeed for the Rb vs PHM OASD, the statistical uncertainty is at the permil level. Up to an averaging time of around 10^4 s, the stability is limited only by the white noise. After that, the OASD first increases as $\tau^{1/2}$ which is characteristic of the frequency random

[2] according to equation (10) of [24]

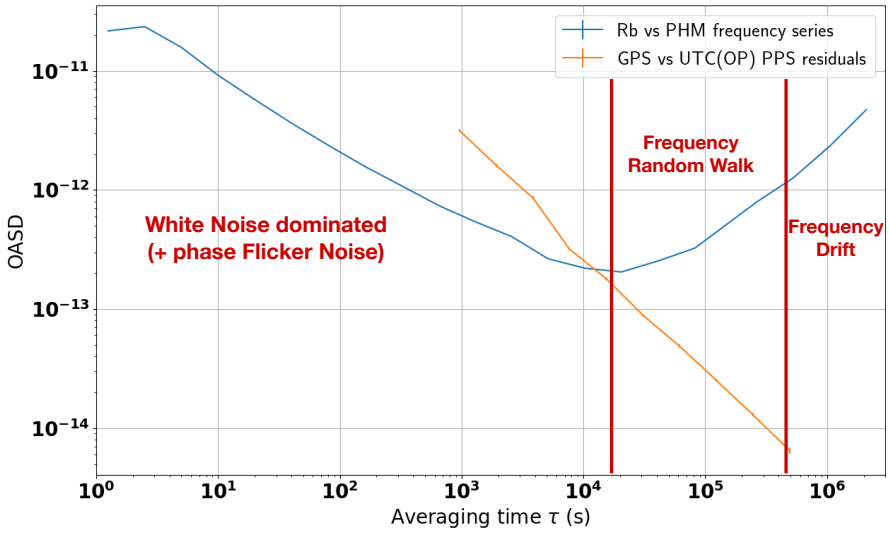

Figure 9. Overlapping Allan Standard Deviation of the Rb/PHM frequency ratio series (in blue), measured by the frequency counter before any correction, and of the GPS signals vs UTC(OP) (in orange) PPS residuals measured by the Septentrio receiver. The main type of noises affecting the Rubidium clock signal stability are indicated where they are limiting the stability.

walk. From $\tau \approx 5 \times 10^5$ s, the OASD increases proportionally to τ. This is characteristic of a deterministic frequency drift which can be easily characterized and corrected for contrary to the frequency random walk. In comparison, the OASD of the GPS signals, estimated using PPS residuals against the UTC(OP) signal that we receive from the SYRTE laboratory via White Rabbit, is only limited by a white noise at least up to an averaging time of 5×10^5 s: the OASD keeps decreasing with the averaging time. At low averaging times, the GPS signals stability is worse than the Rb because of this white noise: the GPS OASD is of around 3×10^{-12} at 960 s compared to around 7×10^{-13} OASD for the Rubidium clock. However, at around 10^4 s, the stability of the Rb signal becomes worse compared to the GPS signals because of the frequency random walk and drift of the Rubidium clock.

In this paper, we used only the GPS satellites with an elevation angle (angle between line of sight and horizontal direction) superior to 15° to extract the Rubidium PPS residuals distribution. During the whole data-taking period, for each data point, the Septentrio receiver picked up an average of 6.5 GPS satellites and at least 4 GPS satellites for each data point. To obtain the Rubidium vs GPS PPS residuals, we take the mean value of the PPS differences between the Rubidium clock and each GPS satellite picked up in the same integration time window of the Septentrio receiver. The obtained PPS residuals is shown in Figure 10. The PPS residuals shown here have already been corrected for the deterministic drift discussed before as this can be easily monitored and corrected for contrarily to the random walk. The correction coefficients will be extracted from this PPS residuals distribution. Before correction, we see that after a few days of data-taking, the Rb PPS can drift away from the GPS signal by more than a hundred nanoseconds because of the random walk noise, hence the need for a correction.

3.1. Offline correction

Figure 11 shows the Allan standard deviation of the Rubidium/PHM frequency ratios measurements. Note that a relative resolution of 10^{-11} was chosen for the frequency measurement with the frequency counter. This is very close to the Phase White Noise of the free running Rubidium so it does not impact significantly the Allan Standard Deviation distribution. The blue distribution shows the result for series corrected only for the deterministic drift of the Rubidium clock, by subtracting the expected time distribution

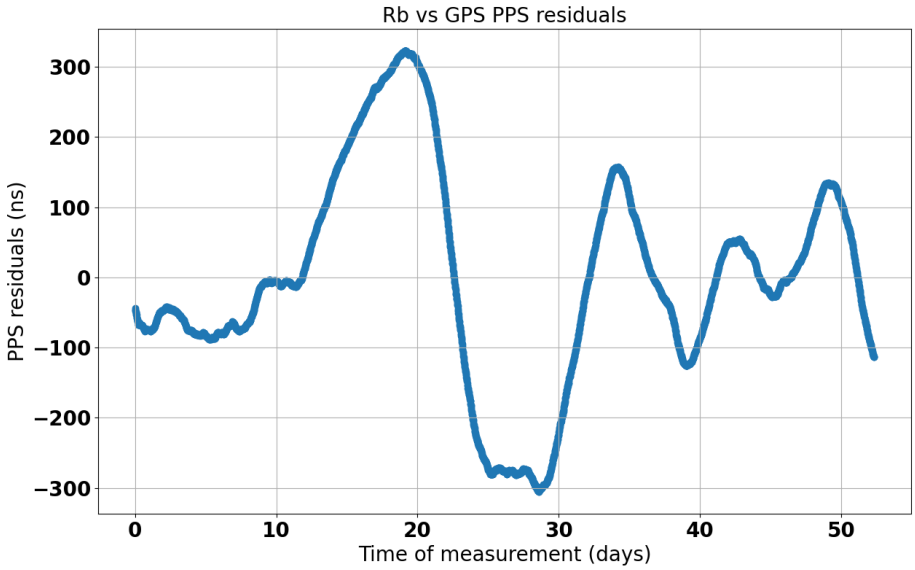

Figure 10. Time distribution of the mean value of the PPS residuals between the Rubidium clock signal and the GPS signals as measured by the Septentrio receiver. The distribution is already corrected for the deterministic drift of the Rubidium clock signal. The large time scale variations are caused by the frequency random walk of the Rubidium clock.

of the series caused by this drift. Note that by correcting the deterministic drift, we also partially correct for the frequency random walk such that the OASD decreases with the averaging times for $\tau > 10^6$ s. In the following, the so-called "uncorrected" distributions are already corrected for this long term drift. The other colors show the results for the series corrected offline, with different width of the correction time window. Here, we use quadratic fits of the Septentrio data (so $a_k \neq 0$ a priori). The shortest time window (2880 s) corresponds to approximately 3 Septentrio integration time windows, so 3 points in the Rb vs GPS PPS residuals distribution. The medium (10560 s) and largest (240, 000 s) correspond respectively to 11 and 250 Septentrio data points.

One sees that with the medium time window compared to the two others, we obtain the best stability at all averaging times. At lower averaging times, the performance is very similar to the uncorrected time series. At higher averaging times, the Allan Standard Deviation is much better than the uncorrected time series and is comparable to the one obtained for the shortest correction time window. This illustrates the fact that both the 2880 s and 10560 s windows are able to correct very well the frequency random walk ($\tau^{1/2}$ component of the ASD) of the uncorrected time series. However, with the shortest correction time window, the short term stability of the time series is degraded compared to the uncorrected series: the value of the ASD at 1 s increases by a factor ~ 1.5. In this scenario, the corrected Rubidium time signal gets very close to the GPS signal which is known to have a higher phase White Noise. Finally, the longest correction time window leads to a similar stability as the shortest one at long term and even poorer stability at $\tau \in [10^4, 10^5]$ s.

Figure 12 shows the Rubidium PPS residuals distribution after the offline correction against the GPS signals. The shorter the correction time window, the better. However, with the medium length time window, we still get a PPS residual lower than 5 ns over the whole data-taking period, which is well below the requirements of HK. With the longest correction time window, jumps of a few tens of nanoseconds are introduced in the time distribution of the PPS residuals. This explains the overall higher ASD: the stability of the signal is limited by those jumps. These jumps can be understood by looking at the fit of the PPS residuals distribution against GPS in this scenario in Figure 13. The time scale of

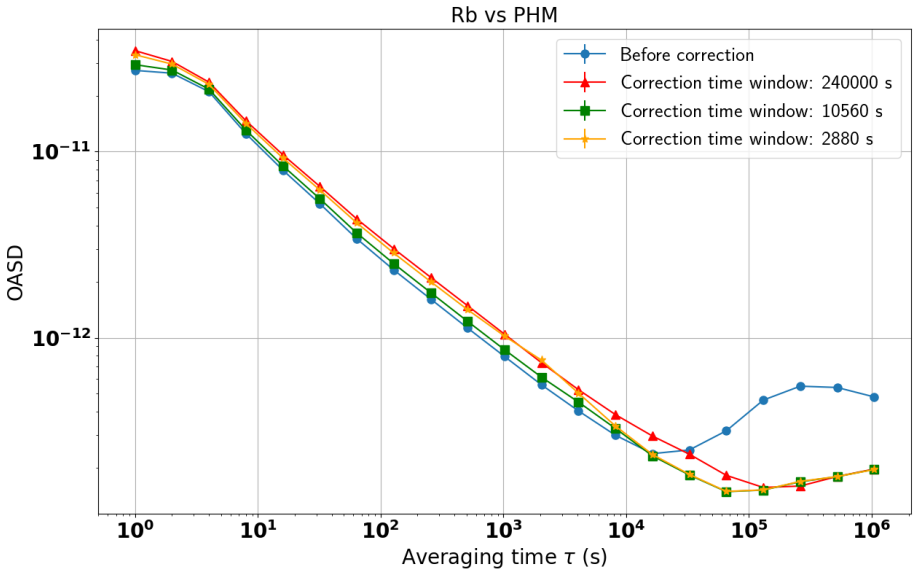

Figure 11. Overlapping Allan Standard deviation of the Rb/PHM frequency ratios series after the deterministic drift correction (in blue) and after the correction from PPS residuals with GPS with a correction time window of 2880 s (orange), 10560 s (green) and 240,000 s (red). The best stability at both short and long averaging times is obtained for the medium time window (10560 s$\approx$ 3 hours).

the variations in the data to fit is too small compared to the 240,000 s time window. In consequence, the fitted tendency from one piece to another is very different and the fitted piece-wise polynomial is not continuous.

With the offline version of the corrections, we thus obtain a very good synchronisation to the GPS PPS signals at the level of a few nanoseconds with the 10560 s time window. However, this version of the correction cannot be applied in real time. In the following paragraphs, we show the results for the online version of the correction that can be applied to correct in real time the time stamps of events in physics experiments.

3.2. Online correction

Figure 14 shows the Allan standard deviation of the uncorrected (blue) and online corrected (other colors) Rubidium/PHM frequency ratios series. The same three time window intervals as in the offline correction scenario are considered. The top panel shows the results using quadratic fits of the Septentrio data and the bottom panel shows the results with linear fits. For the shortest and medium correction time windows, the linear fits lead to better performance with a lower ASD at low averaging times. At 1 s, the ASD with the shortest (medium) correction time window is reduced by a factor 4 (resp. $\sim$ 1.5).

This behavior is very understandable looking at the number of degrees of freedom (number of data points - number of free parameters) in our fits. For the shortest time windows, the number of degrees of freedom is relatively low (0 and 8) in case of quadratic fits so we risk over-fitting to the past data in order to correct the present data. This number of degrees of freedom is not relevant in the offline correction as the fit is performed on the same data as the correction (the over-fitting is not a problem here). Lowering the number of free parameters is one way of increasing the degrees of freedom hence allowing the fit to better generalize to the present data. Another way to increase the number of degrees of freedom is to increase the number of data points in the fit. For the longest time window, there are 247 degrees of freedom in the quadratic fit so we do not risk over-fitting. On the contrary, in that case, quadratic fits lead to a slightly better correction of the random walk that limits the stability only up to $\tau \approx 8 \times 10^4$ s whereas with linear fits, it limits the stability up to $\approx 2 \times 10^5$ s. Note that the degradation of short term stability because of

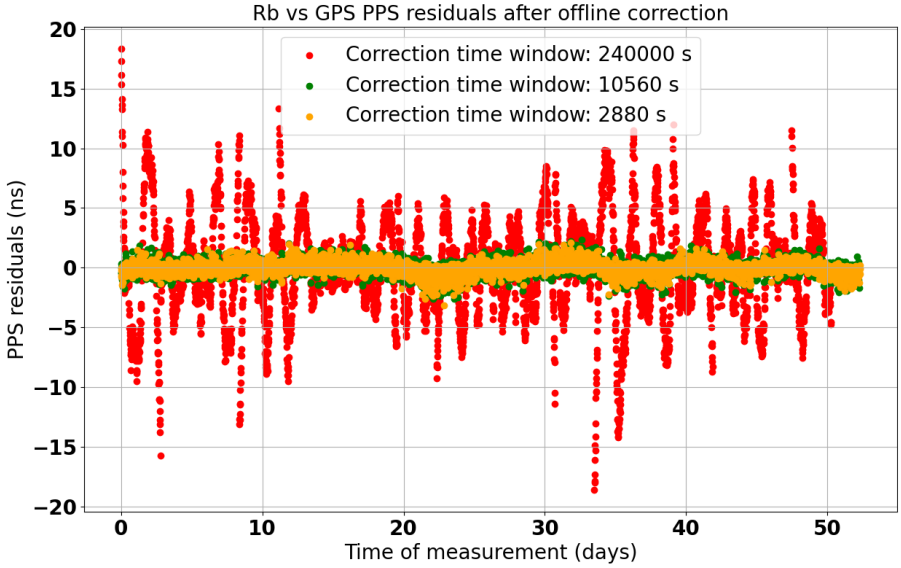

Figure 12. Time distribution of the mean value of the PPS residuals between the Rubidium clock signal and the GPS signals after the offline correction. Three different correction time windows have been tested: 2800 s (orange), 10560 s (green) and 240, 000 s (red).

over-fitting on data from the past is, as expected, also very visible in the OASD of the Rb vs GPS PPS residuals after correction shown in Figure 15. This plot also illustrates that the corrected signal's stability, compared to GPS signals, is not limited by any frequency random walk at least up to an averaging time or 2×10^6 s and correction time window short enough. Indeed, in that case, the OASD keeps decreasing with increasing averaging time.

Regarding the stability of the corrected signals, using linear fits, the conclusions are the same as for the offline correction. The lower Allan Standard deviation, for all averaging times, is achieved with the medium width correction time window. With the shortest time window, the short term stability is degraded, whereas it is the long term stability that is degraded (compared to the other corrected scenarios) with the longest correction time window. Note that, contrary to the offline correction, the online correction with very long time windows does not deteriorate the short term stability of the signal. This is due to the use of "overlapping" windows of Rb vs GPS data. Between two consecutive fits, there is only one data point out of the 250 used that changes (the oldest one from the previous fit is replaced by the newest point). The fit parameters cannot change too abruptly from one fit to another so the resulting distributions are smooth.

If the correction time window is too wide, we cannot correct as well the frequency random walk of the free running Rubidium: the risk is that the Rubidium time signal locally drifts too far away from the UTC. This can be observed in the corrected PPS residuals against GPS in Figure 16 where the maximum residual reaches $\sim$ 60 ns (or $\sim$ 25 ns with quadratic fits) with the 240, 000 s correction time window. With the 10560 s correction time window, the residuals stay in the $\pm$5 ns range. Once again, one can see the reduction of the white noise when using linear instead of quadratic fits for the 2880 s correction time window scenario: the residuals are contained in a $\pm$5 ns range with linear fits instead of $\pm$12 ns with quadratic fits. Note that with linear fits, the difference of OASD at 10^5 s between the longest time window and the others is only of a factor 2.3, and the difference between the shorter time windows and the uncorrected OASD is only a factor 3. Such small differences have a significant impact in terms of synchronisation to the GPS PPS. Before correction, as the reader saw in Figure 10, the free running Rubidium PPS can drift by around 100 ns in 10 days which means that HK's requirmeent for the synchronisation with UTC is not

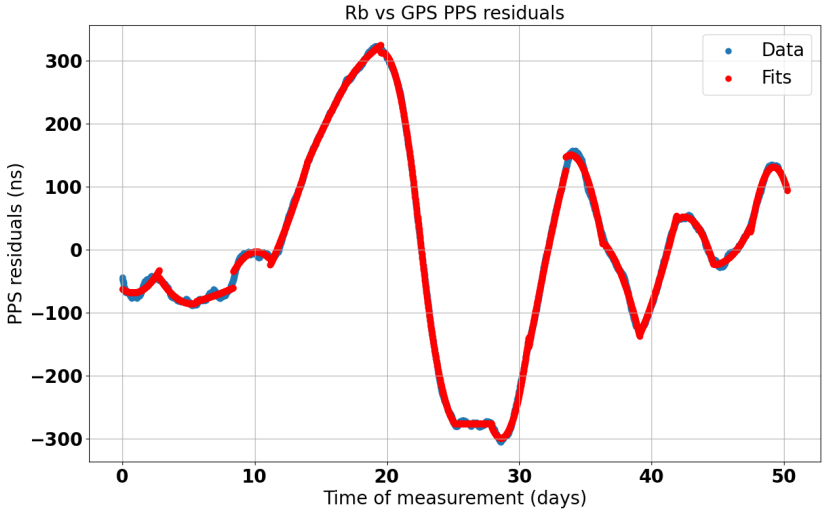

Figure 13. Time distribution of the mean value of the PPS residuals between the Rubidium clock signal and the GPS signals. The red portions show the results of the polynomial fit over consecutive time windows of 240,000 s. The fit sometimes fail to represent the shorter time scales variations of the measured data. The poor fit quality can then lead to introducing jumps in the corrected time signal.

met. After online correction with the longest time window tested, the corrected Rubidium PPS drifts by around 60 ns in a few days whereas with the other time windows because of remaining random walk noise. Even though during the 50 days data-taking period the PPS residuals with respect to GPS signals does not exceed 100 ns, it is not possible to safely claim that the Rubidium PPS drift will not exceed HK's requirement of 100 ns if we use the 240,000 s correction time window. With shorter time windows, this drift seems to be dominated by white noise and is thus contained in a range of a few nanoseconds.

4. Discussion

As advertised before, the advantage of the so-called online correction is that it could be performed in real-time. This is an important feature for applications that necessitate a real-time synchronization with UTC or with another site (like the future HK or DUNE experiments) via a common-view GNSS technique [25]. If a reference clock signal is generated with an atomic clock (like the Rubidium clock used here) and sent to a data acquisition system to be propagated to detectors, one could continuously compare this signal to the GNSS signals using a Septentrio receiver. The correction coefficients a, b and c calculated from the Septentrio data would need to be sent to the data acquisition system so that it could correct the time stamps in real-time.

Figure 17 shows the standard deviation of the Rb vs GPS PPS residuals after correction as a function of the correction time window's width. The performance of the offline and online correction on experimental data (colored dots) is compared to the performance we had obtained on simulated data (colored asterisks) with a correction time window of 10560 s. Note that these simulated data were only taking into account white noises and frequency random walk in the generated PPS signals. No additional uncertainty was added to take into account other types of noise (e.g: flicker noise) or experimental conditions (e.g: imperfect calibrations). These differences can explain the much better performance obtained on simulated data (0.3-0.5 ns) compared to experimental data (0.5-30 ns). For both corrections, very similar performance of synchronization with GPS are obtained for correction time windows below 30,000 s so there is no need to have much shorter windows. This result is consistent with the fact as seen in Figure 9, the stability of the Rubidium signal becomes limited by the frequency random walk for averaging times around 10^4 s. It is also for similar averaging time windows that the Rubidium clock stability becomes worse

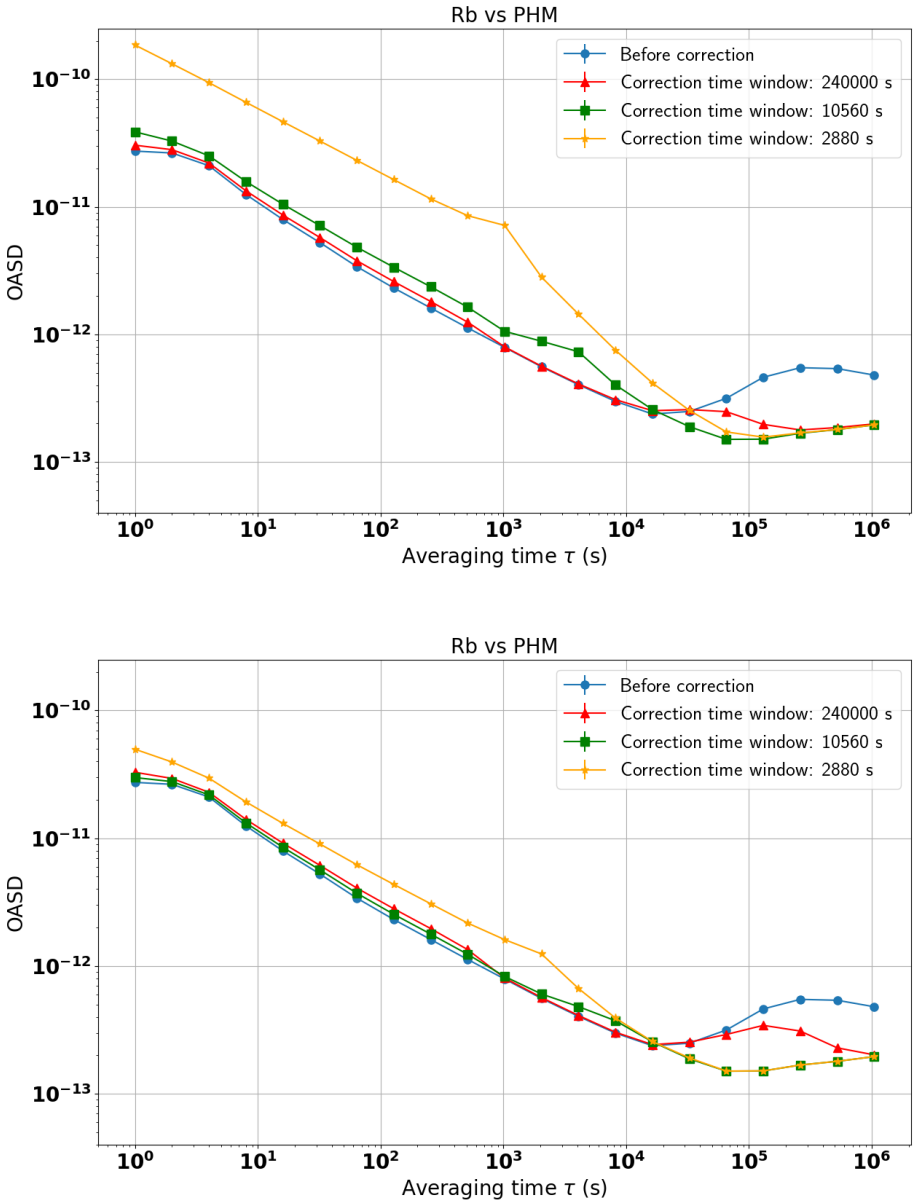

Figure 14. Overlapping Allan Standard deviation of the Rb/PHM frequency ratios series after the deterministic drift correction (in blue) and after the online correction from PPS residuals with GPS with a correction time window of 2880 s (orange), 10560 s (green) and 240,000 s (red). The PPS residuals were fitted with quadratic (top) or linear (bottom) functions of time. A better stability, similar to the offline correction, can be obtained using linear fits.

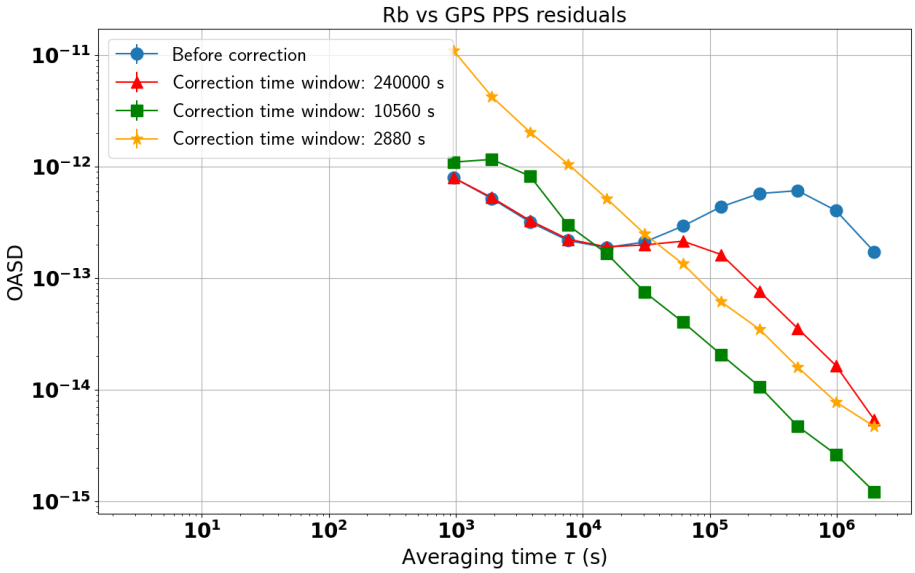

Figure 15. Overlapping Allan Standard Deviation of the Rb vs GPS PPS residuals series after the deterministic drift correction (in blue) and after the online correction with a correction time window of 2880 s (orange), 10560 s (green) and 240,000 s (red). The PPS residuals were fitted with quadratic functions of time. The increase of OASD at 1 s averaging time with decreasing correction time window is consistent with what is observed in the Rb/PHM frequency ratios series after online correction. The less degrees of freedom in the fit, the more we risk over-fitting on past data and lowering the short term stability of the signal.

than the GPS signals. It was thus expected to find that similar correction time windows or shorter ones would be needed to efficiently correct for the random walk. The offline correction seems to provide a slightly better synchronization to GPS (down to 1 ns) but the precision affordable with the online correction is already more than satisfying (better than 5 ns for correction time windows below 100,000 s) for synchronization between several experimental sites. Indeed, the needed level of synchronization is usually of the order of 100 ns for those applications.

5. Conclusions

In this paper, we presented a simple way to use PPS comparisons to GPS signals to correct the time signal generated by a free running Rubidium clock to synchronize it to UTC while preserving its short term stability and correcting the long term frequency random walk. This method has the advantage of using relatively cheap instruments and to be applicable online for a real-time synchronization as well as to be robust against GNSS signal reception failures. The online method could be applied for the real-time synchronization between several experimental sites in physics experiments.

This method consists in fitting the GPS vs Rb PPS residuals measured by a GPS receiver with a piece-wise polynomial function of time and in subtracting the result to the generated time stamps. The method was first designed and validated with simulated signals before assessing its performance on data. We evaluated the performance of this correction by quantifying the stability of the clock signal before and after the correction using the Allan Standard Deviation. We showed that the optimal length of the time window for the fit of the GPS vs Rb PPS residuals seats around 10,000 seconds, corresponding to ~ 10 data points from the receiver. This time window allowed to maintain the best possible short term stability of our generated signal while correcting the drifts caused by the frequency random walk. After correction with this time window, the GPS vs Rb PPS residuals stay within a window of ± 3.5 ns (± 5 ns) for the offline (resp. online) correction during the

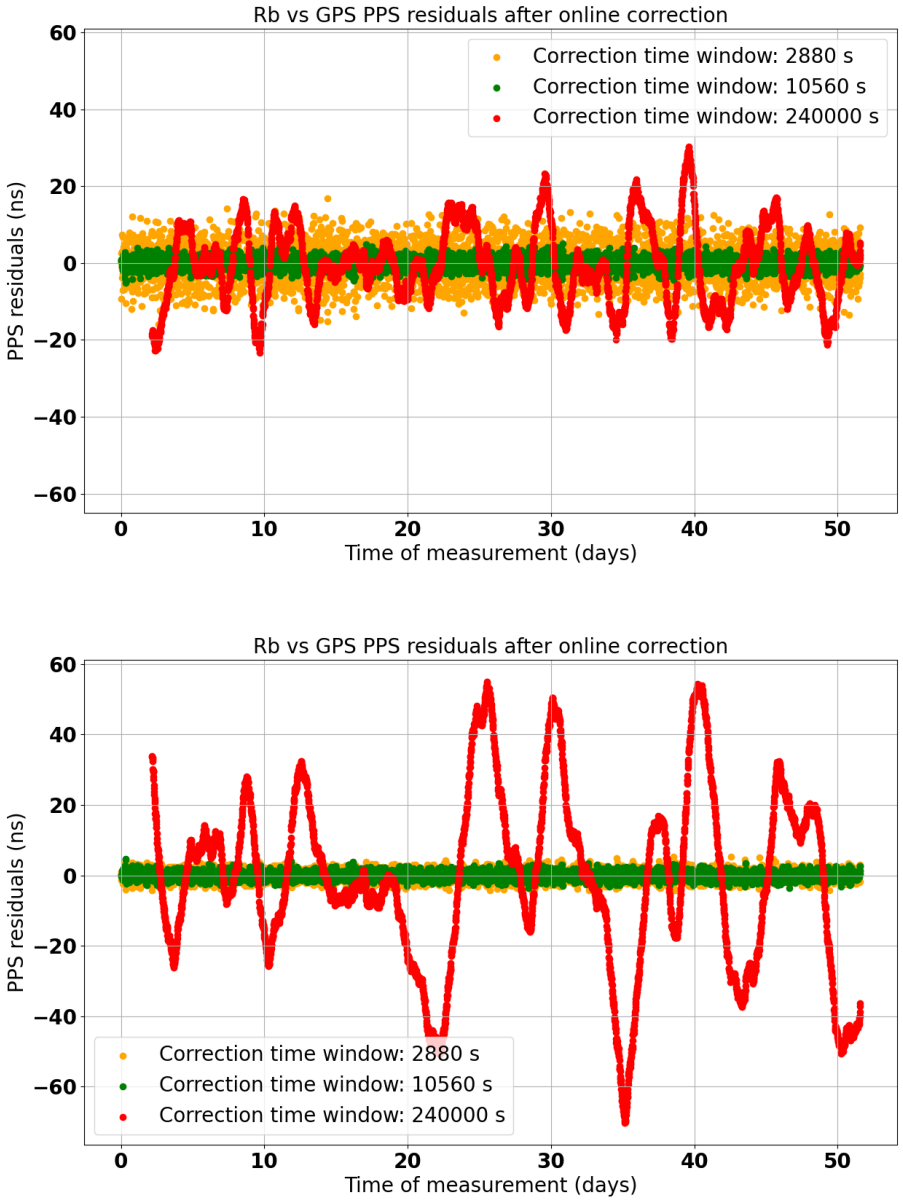

Figure 16. Time distribution of the mean value of the PPS residuals between the Rubidium clock signal and the GPS signals after the online correction. Each point is corrected using a quadratic (top) or linear (bottom) fit of the 2800 s (orange) or 10560 s (green) or 240, 000 s (red) of data points prior to this point. Using linear fits leads to smaller residuals for the shortest time window and bigger ones for the longest time window.

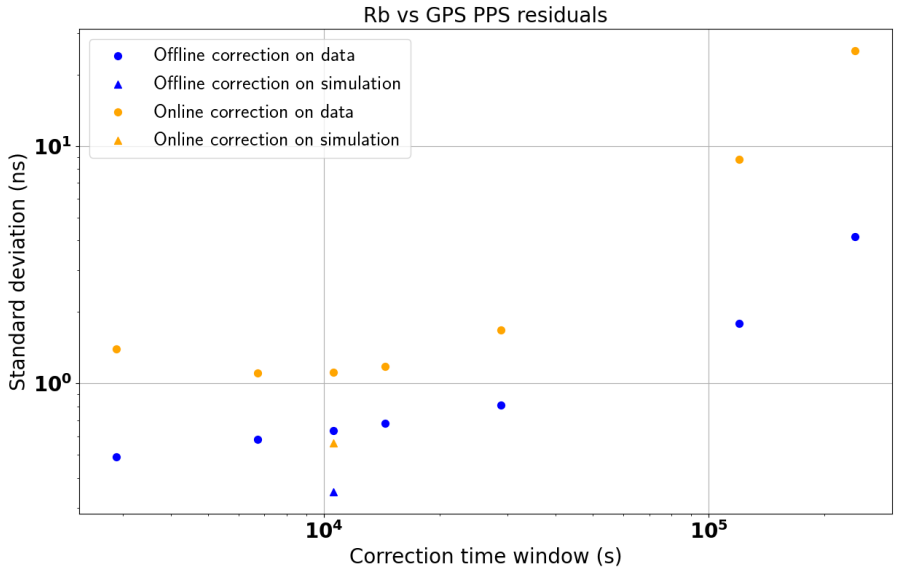

Figure 17. Standard deviation of the residuals distributions between the Rb and the GPS 1 PPS signals after the offline (blue) or online (orange) correction as a function of the correction time window. Quadratic fits of the Septentrio data are used for the offline correction whereas linear fits are used for the online correction. The performance on simulated data is also shown for the 10560 s time window with star markers.

whole $\sim$ 50 days of measurement. This performance largely meets the usual requirements for physics experiments like Hyper-Kamiokande.

Author Contributions: For research articles with several authors, a short paragraph specifying their individual contributions must be provided. The following statements should be used "Conceptualization, X.X. and Y.Y.; methodology, X.X.; software, X.X.; validation, X.X., Y.Y. and Z.Z.; formal analysis, X.X.; investigation, X.X.; resources, X.X.; data curation, X.X.; writing—original draft preparation, X.X.; writing—review and editing, X.X.; visualization, X.X.; supervision, X.X.; project administration, X.X.; funding acquisition, Y.Y. All authors have read and agreed to the published version of the manuscript.", please turn to the CRediT taxonomy for the term explanation. Authorship must be limited to those who have contributed substantially to the work reported.

Funding: Please add: "This research received no external funding" or "This research was funded by NAME OF FUNDER grant number XXX." and and "The APC was funded by XXX". Check carefully that the details given are accurate and use the standard spelling of funding agency names at https://search.crossref.org/funding, any errors may affect your future funding.

Institutional Review Board Statement: In this section, you should add the Institutional Review Board Statement and approval number, if relevant to your study. You might choose to exclude this statement if the study did not require ethical approval. Please note that the Editorial Office might ask you for further information. Please add "The study was conducted in accordance with the Declaration of Helsinki, and approved by the Institutional Review Board (or Ethics Committee) of NAME OF INSTITUTE (protocol code XXX and date of approval)." for studies involving humans. OR "The animal study protocol was approved by the Institutional Review Board (or Ethics Committee) of NAME OF INSTITUTE (protocol code XXX and date of approval)." for studies involving animals. OR "Ethical review and approval were waived for this study due to REASON (please provide a detailed justification)." OR "Not applicable" for studies not involving humans or animals.

Data Availability Statement: We encourage all authors of articles published in MDPI journals to share their research data. In this section, please provide details regarding where data supporting reported results can be found, including links to publicly archived datasets analyzed or generated during the study. Where no new data were created, or where data is unavailable due to privacy or

ethical restrictions, a statement is still required. Suggested Data Availability Statements are available in section "MDPI Research Data Policies" at https://www.mdpi.com/ethics.

Acknowledgments: In this section you can acknowledge any support given which is not covered by the author contribution or funding sections. This may include administrative and technical support, or donations in kind (e.g., materials used for experiments).

Conflicts of Interest: Declare conflicts of interest or state "The authors declare no conflicts of interest." Authors must identify and declare any personal circumstances or interest that may be perceived as inappropriately influencing the representation or interpretation of reported research results. Any role of the funders in the design of the study; in the collection, analyses or interpretation of data; in the writing of the manuscript; or in the decision to publish the results must be declared in this section. If there is no role, please state "The funders had no role in the design of the study; in the collection, analyses, or interpretation of data; in the writing of the manuscript; or in the decision to publish the results".

Abbreviations

The following abbreviations are used in this manuscript:

MDPI	Multidisciplinary Digital Publishing Institute
ASD	Allan Standard Deviation
OASD	Overlapping Allan Standard Deviation
Rb	Rubidium clock
PHM	Passive Hydrogen Maser
GPS	Global Positioning System
UTC	Universal Time Coordinated
GNSS	Global Navigation Satellite Systems
HK	Hyper-Kamiokande
DUNE	Deep Underground Neutrino Experiment
PPS	Pulse Per Second
WR	White Rabbit

Appendix A

References

1. Hyper-Kamiokande Proto-Collaboration, Hyper-Kamiokande Design Report. *arXiv:1805.04163*, 2018.
2. M. Guler *et al.*, OPERA: An appearance experiment to search for nu/mu <–> nu/tau oscillations in the CNGS beam. Experimental proposal, CERN-SPSC-2000-028;
3. K. Abe *et al.*, The T2K Experiment, Nucl. Instrum. Meth. A **659** (2011), 106-135, doi:10.1016/j.nima.2011.06.067, [arXiv:1106.1238 [physics.ins-det]].
4. D.S. Ayres *et al.*, The NOvA Technical Design Report, (2007), doi:10.2172/935497
5. B. Abi *et al.*, Deep Underground Neutrino Experiment (DUNE), Far Detector Technical Design Report, Volume I: Introduction to DUNE, *arXiv:2002.02967*, 2020.
6. Mészáros, P., Fox, D.B., Hanna, C. et al. Multi-messenger astrophysics. Nat Rev Phys 1, 585–599 (2019). https://doi.org/10.1038/s42254-019-0101-z
7. The Supernova Early Warning System web page. https://snews2.org/.
8. T2K collaboration, Upper bound on neutrino mass based on T2K neutrino timing measurements,Physical Review D (93),2016, DOI: 10.1103/PhysRevD.93.012006, https://arxiv.org/abs/1502.06605
9. SK collaboration, The Super-Kamiokande detector, Nuclear Instruments and Methods in Physics Research Section A: Accelerators, Spectrometers, Detectors and Associated Equipment(501), 2003, https://doi.org/10.1016/S0168-9002(03)00425-X.
10. Mellet, L.; Guigue, M.; Popov, B.; Russo, S.; Voisin, V., on behalf of the Hyper-Kamiokande Collaboration. Development of a Clock Generation and Time Distribution System for Hyper-Kamiokande. Phys. Sci. Forum 2023, 8, 72. https://doi.org/10.3390/psf2023008072.
11. Lombardi, M. Fundamentals of Time and Frequency. In The Mechatronics Handbook ; CRC Press: Boca Raton, FL, USA , 2002; ISBN 978-0-8493-6358-0.
12. Giulia Brunetti. Neutrino velocity measurement with the OPERA experiment in the CNGS beam. Other [cond-mat.other]. Université Claude Bernard - Lyon I; Università degli studi (Bologne, Italie), 2011. English. ⟨NNT : 2011LYO10088⟩. ⟨tel-00843100⟩
13. Howe, D.A.; Allan, D.U.; Barnes, J.A. Properties of signal sources and measurement methods. In Proceedings of the Thirty Fifth Annual Frequency Control Symposium, Philadelphia, USA, 27-29 May 1981.
14. Serrano, J. et al., The White Rabbit project, 2013. https://cds.cern.ch/record/1743073

15. Daniluk, G, White Rabbit calibration procedure (version 1.1), 2015. https://white-rabbit.web.cern.ch/documents/WR_Calibration-v1.1-20151109.pdf
16. E. Cantin et al., "REFIMEVE Fiber Network for Time and Frequency Dissemination and Applications," 2023 Joint Conference of the European Frequency and Time Forum and IEEE International Frequency Control Symposium (EFTF/IFCS), Toyama, Japan, 2023, pp. 1-4, doi: 10.1109/EFTF/IFCS57587.2023.10272084.
17. C. B. Lim et al., "Extension of REFIMEVE with a White Rabbit Network," 2023 Joint Conference of the European Frequency and Time Forum and IEEE International Frequency Control Symposium (EFTF/IFCS), Toyama, Japan, 2023, pp. 1-4, doi: 10.1109/EFTF/IFCS57587.2023.10272069.
18. Defraigne, P.; Petit, G. CGGTTS-Version 2E: an extended standard for GNSS Time Transfer, Metrologia (52), IOP Publishing, 2015, DOI: 10.1088/0026-1394/52/6/G1
19. Mellet,L. From T2K to Hyper-Kamiokande : neutrino oscillation analysis and preparation of the time synchronization system. 2023, ⟨NNT : 2023SORUS297⟩. ⟨tel-04284182⟩
20. Plumb, John et al. Absolute calibration of a geodetic time transfer system. Ultrasonics, Ferroelectrics and Frequency Control, IEEE Transactions on (2005) **52**, 1904-1911 doi = 10.1109/TUFFC.2005.1561658
21. J. A. Barnes et al., "Characterization of Frequency Stability," in IEEE Transactions on Instrumentation and Measurement, vol. IM-20, no. 2, pp. 105-120, May 1971, doi: 10.1109/TIM.1971.5570702.
22. T. J. Witt, "Using the Allan variance and power spectral density to characterize DC nanovoltmeters," in IEEE Transactions on Instrumentation and Measurement, vol. 50, no. 2, pp. 445-448, April 2001, doi: 10.1109/19.918162.
23. D. W. Allan, "Statistics of atomic frequency standards," in Proceedings of the IEEE, vol. 54, no. 2, pp. 221-230, Feb. 1966, doi: 10.1109/PROC.1966.4634.
24. W.J. Riley. Handbook of frequency stability analysis. NIST Special publication 1065. July 2008.
25. Weiss, M.A.; Petit, G.; Jiang, Z. A comparison of GPS common-view time transfer to all-in-view. In Proceedings of the IEEE International Frequency Control Symposium and Exposition, 2005.
26. https://webapp.csrs-scrs.nrcan-rncan.gc.ca/geod/tools-outils/ppp.php